Pre-Print Manuscript of Article:
Bridgelall, R., "Inertial Sensor Sample Rate Selection for Ride Quality Measures," *Journal of Infrastructure Systems*, American Society of Civil Engineering, 21 (2), pp. 1-5, 2014.

Inertial Sensor Sample Rate Selection for Ride Quality Measures

Raj Bridgelall, Ph.D.[1]

Abstract

The Road Impact Factor is a measure of ride-quality. It is derived from the average inertial response of vehicles to road roughness. Unlike the International Roughness Index, the most common measure, the road impact factor does not rely on specialized instrumentation to measure spatial deviations from a flat profile. The most significant advantage of the Road Impact Factor is that low-cost sensors distributed in smartphones and connected vehicles generate the measurements directly. Standardizing the sample rate of inertial sensors in vehicles will provide consistent measures at any speed. This study characterizes the impact of sample rate and traversal volume on measurement consistency, and conducts case studies to validate the theories developed for a recommended standard at 64 hertz.

CE Database subject headings: Deterioration; Forecasting; Frequency response; Intelligent transportation systems; Pavement management; Preservation; Probe instruments; Spectral analysis; Surface roughness; Vibration

Author Keywords: Ride quality; Smartphone sensors; Road Impact Factor; International Roughness Index

[1]Assistant Professor of Transportation and Program Director, Center for Surface Mobility Applications & Real-Time Simulation environments (SMARTSe[SM]), Upper Great Plains Transportation Institute, North Dakota State University, P.O. Box 863676, Plano, TX 75086. Phone: 408-607-3214, E-mail: raj@bridgelall.com

Introduction

Transportation agencies in rural areas face the enormous challenges of accurately forecasting pavement deterioration and assuring consistent repair quality without disrupting traffic flows. Maintaining a state of good repair requires continuous and consistent performance measures, especially in regions where roads deteriorate rapidly, such as rural freight corridors and oilfields. The Federal Highway Administration (FHWA) requires annual reporting of the International Roughness Index (IRI), the most common measure of ride quality for the National Highway System (HPMS 2012). However, transportation agencies do not regularly monitor the ride quality of repaired and local roads because of the high complexity and cost of producing the IRI.

To provide continuous, network-wide, and lower-cost ride-quality measures, the author developed and validated a new approach called the Road Impact Factor (RIF). It is derived directly from inertial sensors onboard vehicles (Bridgelall 2014a). The emerging dominance of mobile device applications (apps), social media, and connected vehicles presents significant opportunities for the ubiquitous deployment of wireless sensors to monitor and report ride quality through cloud computing. An additional benefit of the RIF is its direct proportionality to the IRI as demonstrated in previous case studies (Bridgelall 2014a). This was also demonstrated in a previous publication (Bridgelall 2014b) by deriving the ratio of the RIF and the IRI for the same quarter-car impulse response. To standardize the approach for consistent RIF measures across all vehicle types, inertial sensors must use the same sample rate. Selecting the minimum sample rate that captures all the roughness energy from any vehicle will minimize power and data storage requirements. This study characterizes the RIF variability with sample rate and traversal volume, and validates the relationship through case studies.

This is the first study to characterize the trade-off between inertial sensor sample rate, traversal volume, and RIF variance. Related studies utilize inertial data to correct for reference plane variations in laser-based road profilers (Hegmon 1992), to estimate the profile of a terrain (Ward and Iagnemma 2009), and to evaluate vehicle dynamics across different terrain types (Dawkins 2011). Those studies utilized the highest sample rate achievable by the inertial sensors available at the time.

This paper is organized as follows: the next section reviews the RIF model and its associated speed-independent transform called the time-wavelength intensity transform (TWIT). The third section introduces a frequency response model to identify a vehicle's modal resonance parameters from sampled inertial data and to relate signal energy to sample rate. The fourth section develops a theoretical relationship between the RIF variance, signal energy, and traversal volume. The fifth section presents case studies that validate the models by quantifying the RIF margin-of-error (MOE) for three distinct pavement roughness categories. The final section summarizes and concludes the study.

Roughness Evaluation Model

Previous research (Bridgelall 2014a) defined the RIF, denoted $R^L[p]$, as the g-force per meter (g/m) sensed when traversing a road segment of length L, during time-period p where:

$$R^L[p] = \sqrt{\frac{1}{L}\int_0^{L/\bar{\sigma}} \left| g_z(t)\sigma(t) \right|^2 dt} \tag{1}$$

The instantaneous traversal speed is $\sigma(t)$ and the vertical acceleration output from the sensor is $g_z(t)$. The corresponding TWIT is speed-independent. It is a linear combination of the average RIF from each speed band where the coefficients are the percentages of vehicle traversals for

each band. The TWIT for a road segment *k* during an arbitrary time-interval ΔP of time-index *j* is denoted $\Psi_k[\Delta P_j]$ where:

$$\Psi_k(\Delta P_j) = \frac{\sum_{w=1}^{B_k} \overline{R}_{\Delta\sigma_w}^{\Delta P_j}[k] \times N_{\Delta\sigma_w}^{\Delta P_j}[k]}{\sum_{w=1}^{B_k} N_{\Delta\sigma_w}^{\Delta P_j}[k]} \tag{2}$$

The speed-band or window size is $\Delta\sigma$ and the window index is *w*. The average RIF of vehicles traversing segment *k*, within a speed band $\Delta\sigma_w$, and during time increment ΔP_j is denoted as $\overline{R}_{\Delta\sigma_w}^{\Delta P_j}[k]$. The corresponding traversal volume is denoted as $N_{\Delta\sigma_w}^{\Delta P_j}[k]$. The total number of speed bands available for segment *k* is B_k. A key property of the TWIT is that it emphasizes roughness from longitudinal profile wavelengths that the vehicle population experiences at the most common speed ranges.

Vehicle Response Energy

Road roughness excites the vibration modes of a moving vehicle. The damped mass-spring model for each wheel-suspension assembly or "quarter-car" includes a series combination of sprung and unsprung masses that represent the body suspension and wheel components respectively. A pair of second-order differential equations characterizes each model. Their solution identifies the dominant resonant frequencies and damping ratios of each mode as functions of the vehicle body mass, wheel mass, spring constants, and damping coefficients (Angeles 2011). These physical parameters must be known to determine the characteristics of each quarter-car mode. The vertical acceleration at the sensor location is the vector sum of responses from roughness excitation at each quarter-car. To characterize the roughness energy from vehicle vibrations, the Nyquist Theorem (Oppenheim and Schaefer 1975) dictates that a

sensor must sample the motion response at a rate that is at least twice that of the highest mode frequency. The vertical acceleration responses from road roughness typically contain an insignificant amount of energy above the damped tire resonance frequency.

It is standard practice for vehicle manufacturers to attenuate the suspension motion between 4 and 8 hertz because vibration levels within that frequency range are the most harmful to humans (Griffin 1990). To achieve this, suspension system engineers design the sprung mass resonant frequency between 0.9 and 1.5 hertz for all vehicle types (General Motors 1987). Consequently, the unsprung mass resonance frequencies are typically about ten times higher than those of the sprung mass modes (Gillespie 2004).

This research finds that it is analytically convenient to identify the dominant resonance frequencies and their damping ratios by decomposing the composite inertial spectrum into individual quarter-car systems as illustrated in Fig. 1. The Discrete Fourier Transform (DFT) of the sensor signal characterizes the frequency response of the sensor and the aggregate responses from n quarter-cars. Modeling the DFT as a modulation of the sensor response with a linear combination of responses from each damped mass-spring system produces an estimate of their resonance frequencies and damping ratios. Suitable linear programming techniques can identify the linear combination coefficients and the model parameters that minimize the estimate error. The second-order low-pass filters (LPFs) are Fourier Transforms of the impulse responses of under-damped mass-spring systems. The resonant frequencies of the sprung and unsprung mass modes of each quarter-car contribution are $f_{[s,n]}$ and $f_{[u,n]}$ hertz respectively. Their corresponding damping ratios are respectively $\zeta_{[s,n]}$ and $\zeta_{[u,n]}$. Hence, the magnitude spectrum of the composite transfer function $G_z(f)$ as a function of frequency f is:

$$G_z(f) = \gamma_g(f) \sum_{n=1}^{W} \sum_{m=1}^{2} \frac{\beta_{[m,n]}}{4\pi^2} \sqrt{\frac{1}{1-\zeta_{[m,n]}^2}} \frac{1}{\sqrt{\left(\left[f_{[m,n]}^2 - f^2\right]^2 + \left[2\zeta_{[m,n]} f_{[m,n]} f\right]^2\right)}} \tag{3}$$

where W is the number of wheel-spring assemblies, and the subscripts $m = 1$ and $m = 2$ enumerate the sprung (s) and unsprung (u) mass-spring system parameters respectively. The sensor function $\gamma_g(f)$ is a second derivative operator, and the coefficients of the LPF linear combination are $\beta_{[m,n]}$.

A vehicle traveling a segment of length L at a constant speed $\bar{\sigma}$ will produce a finite time signal with longitudinal energy density E_{gz}^L. Sampling the time-limited signal $g_z(t)$ produces a vector $g_z[k]$ with samples at time instants k. From Parseval's Theorem (Chen 2004):

$$E_{gz}^L = \frac{1}{L} \sum_{k=0}^{N-1} \left|g_z[k]\right|^2 = \frac{1}{NL} \sum_{k=0}^{N-1} \left|G_z[k]\right|^2 \tag{4}$$

where $G_z[k]$ is the DFT of $g_z[k]$. At a sample rate of f_s both vectors contain $(L/\bar{\sigma})f_s = N$ samples of the signal plus noise. The sample error sequence, e_n includes quantization noise, electronic noise, and wheel-path variations among traversals. The noise energy N_κ is:

$$N_\kappa = E\left\langle e_{[n,\kappa]}^2 \right\rangle \frac{1}{f_s} \tag{5}$$

where $E\left\langle e_{[n,\kappa]}^2 \right\rangle$ is the expected value of the squared sample-errors or equivalently the noise power (Skylar 2009) for traversal κ. For a given sample rate f_s the variance of the signal energy among traversals is equivalent to the variance of the noise energy among traversals where:

$$Var\left[E_{gz}^L\right] = Var\left[N_\kappa\right] = Var\left[\frac{E\left\langle e_{[n,\kappa]}^2 \right\rangle}{f_s}\right] = \frac{1}{f_s^2} Var\left[E\left\langle e_{[n,\kappa]}^2 \right\rangle\right] \tag{6}$$

This expression shows that increasing the sampling rate decreases the signal variance, thereby improving the consistency of the sampled signal energy from one traversal to the next.

RIF Variance

The RIF for a segment of length L, traveled at a mean speed $\overline{\sigma}_\kappa$ for the κ^{th} traversal is:

$$R_{\overline{\sigma}}^{L} = \overline{\sigma}_\kappa \sqrt{\frac{1}{L}\int_0^{L/\overline{\sigma}} \left|g_z(t)\right|^2 dt} = \overline{\sigma}_\kappa \sqrt{E_{gz}^{L}} \tag{7}$$

From the theory of error propagation (Ku 1966), the standard deviation of the RIF, s_{RIF}^{L} is:

$$s_{RIF}^{L} = \sqrt{\left(\frac{\partial R_{\overline{\sigma}}^{L}}{\partial \overline{\sigma}_\kappa}\right)^2 Var\left[\overline{\sigma}_\kappa\right] + \left(\frac{\partial R_{\overline{\sigma}}^{L}}{\partial E_{gz}^{L}}\right)^2 Var\left[E_{gz}^{L}\right] + \left(\frac{\partial R_{\overline{\sigma}}^{L}}{\partial \overline{\sigma}_\kappa}\right)\left(\frac{\partial R_{\overline{\sigma}}^{L}}{\partial E_{gz}^{L}}\right) s_{\overline{\sigma}E}^2} \tag{8}$$

where $Var\left[\overline{\sigma}_\kappa\right]$ is the variance of the mean speed among traversals. The covariance of the mean speed and the vertical acceleration signal energy is denoted $s_{\overline{\sigma}E}^2$. The random variables for mean speed and vertical acceleration signal energy are independent; therefore, the covariance factor must be zero. Evaluating the partial derivatives indicated in Equation (8) and substituting the noise energy factor from Equation (5) yields:

$$s_{RIF}^{L} = \sqrt{\overline{E}_{gz}^{L} Var\left[\overline{\sigma}_\kappa\right] + \frac{\left(\overline{\sigma}_{Nt}/2\right)^2}{\overline{E}_{gz}^{L}} Var\left[E\left\langle e_{[n,\kappa]}^2 \right\rangle\right] \frac{1}{f_s^2}} \tag{9}$$

where $\overline{E}_{gz}^{L}$ and $\overline{\sigma}_{Nt}$ are the averages of the vertical acceleration signal energy and the mean speed among traversals. Hence, the RIF variance among traversals increases when the variance of the mean traversal speed increases, but decreases when the sample rate increases. The RIF MOE for a (1-α)% confidence interval with significance α is the inverse power function (Papoulis 1991):

$$MOE_{RIF} = \frac{s_{RIF}^{L} \times t_{1-\alpha/2,df}}{\sqrt{N_{\upsilon}}} \tag{10}$$

where N_{υ} is the traversal volume, and $t_{1-\alpha/2}$ is the t-distribution with degrees of freedom (*df*), which equals $N_{\upsilon} - 1$.

Case Study

Three sedans of different sizes, a large van, and a sports utility vehicle (SUV) provided affordable and convenient platforms to collect data for all case studies. The sedans were a Toyota Camry LE 2007, a Subaru Legacy 2007, and a Ford Contour 1995. The van was a Ford E350 2011 and the SUV was a Ford Explorer 2001. The sprung and unsprung mass responses for all vehicles were between 1 and 2 hertz, and 11 and 20 hertz respectively. As indicated in previous work, automotive engineers design the suspension responses of all standard roadway vehicles to be similar because of the need to provide a consistent human ride comfort (Bridgelall 2014b).

The author developed a custom iOS® data logger application (app) to run on any Apple iPhone model that includes a global positioning system (GPS) receiver of any type, and at least one accelerometer. The specific model used was an iPhone 4S with iOS Version 7.1 and 8 GB memory. The GPS receiver sampled at a default rate of approximately one hertz. The app provided a form to select the accelerometer sample rate from 1 hertz to 128 hertz inclusive. To compare the RIF at different sample rates, the author used the same Subaru Legacy sedan with the smartphone secured flat onto the dashboard.

Frequency Response

A vertical acceleration signal is sampled at 128 hertz using a Toyota Camry 2007 LE sedan equipped with an inertial sensor. Fig. 2 shows the DFT of the sampled signal (solid line). The dotted line is a least squares fit of Equation (3) with W=1 for the response range from 0.1 to 20 hertz. The coefficient of determination for this fit is 91.8%. The model indicates that the sprung and unsprung mass modes are in the vicinity of 1.8 and 12 hertz respectively, with corresponding damping ratios of approximately 0.3 and 0.1. It is evident that there are several peaks in the region of each dominant mode. Those are because of harmonics produced when the quarter-cars of each axle crosses the same bump (Bridgelall 2014b). For this estimate, the ratio of the unsprung mass to the sprung mass LPF amplitude coefficient is approximately 5.7.

Margin-of-Error

The segment of Bolley Drive on the North Dakota State University campus, shown in Fig. 3, contains a two-track rail grade crossing that produces a noticeably rougher ride than the rest of the segment. The crossing consists of four rails. The 50 meter segment north of the crossing is significantly rougher than the 50 meter segment south of the crossing. However, the north segment is much smoother than the 50 meter segment containing the crossing. To quantify and compare the roughness of these road segments, the driver maintained a speed of approximately 7 $m \cdot s^{-1}$ throughout all segments. The smartphone app logged the inertial sensor $g_z[k]$ output by sampling at rates of approximately 1, 2, 4, 8, 16, 32, 64, and 93 hertz. For each sample rate, Table 1 lists the averages and standard deviations of the RIF from 28 traversals. Two outlier data logs from each set of 30 traversals were removed. Fig. 4 plots the average RIF. For all sample rates, the relative differences in roughness for each segment corresponded to roughness differences that the driver perceived. As expected, the roughness measure generally stabilized as

the sample rate increased beyond 32 hertz, which is about twice the unsprung mass resonance of the vehicle. Similarly, the trend in Table 1 shows that the standard deviations of the roughness measure generally decreased as the sample rate increased.

Fig. 5 plots the MOE as a percentage of the mean RIF. This implies that equal magnitude RIF variations will appear as larger percentages for a lower RIF values than for a higher ones. For example, the RIF standard deviation is approximately 0.05 g/meter for each of the road segments sampled at 32 hertz. However, their corresponding MOEs are 10% for the smooth segment with an average RIF of 0.16 g/meter, but only 4% for the rail-grade segment with a much higher average RIF of 0.57 g/meter. As anticipated from Equation (9), the MOE for all roughness categories declined as the sample rate increased. Increasing the sample rate beyond twice the dominant mode frequency provided diminishing returns in MOE reduction. The RIF standard deviation measured from all sample rate data sets was within 5% of the theoretical value predicted by Equation (9). The average of the mean traversal speed $\overline{\sigma}_{\kappa}$ and its standard deviation across $\kappa = 28$ traversals was 7.15 $m \cdot s^{-1}$ and 0.45 $m \cdot s^{-1}$ respectively.

From the central-limit-theorem (Papoulis 1991) and Equation (10), the variability of the mean RIF diminishes with increasing traversals. Fig. 6 plots the MOE as a function of the traversal volume across a 200 meter section of Bolley Drive that includes all three segments. For sample rates of at least 64 hertz, the MOE drops below 5% after only 6 traversals. In general, as the traversal volume increased, the MOE diminished more slowly for higher sample rates than for the lower sample rates. This is because a higher sample rate reduces the noise energy, per Equation (5), thereby improving the signal consistency from one traversal to the next. The trend in error reduction with traversal volume is an inverse power function that closely approximates Equation (10).

Summary and Conclusions

When using the RIF, a fixed sample rate for inertial sensors will provide consistent characterization of ride quality across all vehicle types. The minimum sample rate should be at least twice the highest dominant mode of all vehicles traversing the segment. It is analytically convenient to estimate the suspension system model parameters directly from the vertical acceleration signal samples when the sprung and unsprung masses and spring constants are unknown. Given that standard design practices attenuate suspension responses to excitation frequencies above approximately 32 hertz, the sample rate recommended for standardization is 64 hertz.

The case study demonstrated that the RIF margin-of-error diminishes asymptotically when the sample rate increases beyond this recommended frequency. The RIF variance decreases when the signal sample rate increases. However, increasing the sample rate beyond 64 hertz provides diminishing returns in RIF consistency. Given a sample rate and speed variance, the RIF variability diminishes as the inverse square-root of the traversal volume. Therefore, the traversal volume needed for a desired level of RIF accuracy is proportional to the square of the RIF standard deviation.

Future work will use the theoretical framework developed here to characterize the accuracy of models that can incorporate the RIF to forecast pavement deterioration and vehicle operating costs. The RIF can also estimate the location of pavement distress symptoms. Therefore, future work will characterize symptom location accuracy in terms of vehicle suspension parameter variations and errors in geospatial position estimates.

Acknowledgement

This work is based on research supported by the United Stated Department of Transportation (USDOT), Research and Innovative Technology Administration (RITA) under the Rural Transportation Research Initiative.

Notation

The following symbols are used in this paper:

$A_{LP[n]}$ = low-pass filter amplitude for quarter-car n;

B_k = number of speed bands available for segment k;

E_{gz}^{L} = vertical acceleration signal energy per length of road;

$\overline{E}_{gz}^{L}$ = average of the vertical acceleration signal energy among traversals;

$e_{[n,\kappa]}$ = sampled signal error (noise) for traversal κ;

f = frequency in hertz;

f_s = signal sample rate in hertz;

$f_{[c,n]}$ = low-pass filter cut-off frequency for quarter-car n;

$f_{[s,n]}$ = sprung mass resonance mode frequency;

$f_{[u,n]}$ = unsprung mass resonance mode frequency;

$g_z(t)$ = g-force output from a vertical acceleration sensor as a function of time t;

$G_z(f)$ = magnitude spectrum of the vehicle inertial response;

L = length of road segment;

N_κ = noise energy random variable for traversal κ;

N_v = the traversal volume;

$N_{\Delta\sigma_w}[k]$ = number of vehicles traveling across segment k, within speed band $\Delta\sigma_w$;

$N^{\Delta P_j}[k]$ = number of vehicles traveling across segment k, within time-period ΔP_j;

ΔP_j = time-period increment of instance j;

$R^L[p]$ = RIF for segment of length L evaluated in time-period p;

$\overline{R}^{\Delta P_j}[k]$ = average RIF for segment k, within time-period ΔP_j;

$\overline{R}_{\Delta\sigma_w}[k]$ = average RIF for segment k, within speed band $\Delta\sigma_w$;

$R^L_{\overline{\sigma}}$ = RIF for segment of length L when traversed at an average speed $\overline{\sigma}$;

s^L_{RIF} = standard deviation of the RIF for segment of length L;

$s^2_{\overline{\sigma}E}$ = covariance of the average speed and vertical acceleration signal energy;

T = total traversal time across a segment;

$t_{1-\alpha/2,df}$ = t-distribution with α significance and df degrees of freedom;

$U(t)$ = the Heaviside step function;

$\alpha_{[u,n]}$ = proportion of each LPF in the parallel filter model;

$\Delta\sigma_w$ = speed band window size and instance w;

γ_g = inertial sensor function;

$\overline{\sigma}_\kappa$ = mean or constant speed for traversal κ;

$\overline{\sigma}_{Nt}$ = average of the mean speed for all traversals;

$\sigma(t)$ = instantaneous traversal speed as a function of time;

$\Psi_k(\Delta P_j)$ = TWIT for time-period increment instance j;

$\zeta_{[s,n]}$ = damping ratios of the sprung mass frequency response;

$\zeta_{[u,n]}$ = damping ratios of the unsprung mass frequency response.

References

Angeles, Jorge. *Dynamic Response of Lineaer Mechanical Systems: Modeling, Analysis and Simulation.* New York: Sringer, 2011.

Bridgelall, Raj. "Connected Vehicle Approach for Pavement Roughness Evaluation." *Journal of Infrastructure Systems* (American Society of Civil Engineers) 20, no. 1 (March 2014): 04013001.

Bridgelall, Raj. "A participatory sensing approach to characterize ride quality." *Proc. SPIE* 9061, Sensors and Smart Structures Technologies for Civil, Mechanical, and Aerospace Systems 2014, 90610A (March 8, 2014).

Chen, Chi-Tsong. *Signals and Systems.* 3rd. New York: Oxford University Press, 2004.

Dawkins, Jeremy James. *Terrain Characterization and Roughness Estimation for Simulation and Control of Unmanned Ground Vehicles.* PhD Thesis, Auburn, Alabama: Auburn University, 2011.

General Motors. *Suspension Rates and Frequency.* Suspension Design Guidelines 1070, Detroit, Michigan: General Motors, 1987.

Gillespie, Thomas D. *CarSim Data Manual.* Ann Arbor, Michigan: Mechanical Simulation Corporation, 2004.

Griffin, M. J. *Handbook of Human Vibration.* New York: Elsevier, 1990.

Hegmon, R. R. "Some Results from Ongoing Research on Road Roughness." *Vehicle, Tire, Pavement Interface.* Santa Barbara, CA: American Society for Testing and Materials, 1992. 16-17.

HPMS. Highway Performance Monitoring System Field Manual (HPMS), Office of Highway Policy Information Federal Highway Administration, Washington, DC: Federal Highway Administration, 2012.

Ku, Harry H. "Notes on the Use of Propagation of Error Formulas." *Journal of Research of the National Bureau of Standards, Section C: Engineering and Instrumentation* (National Bureau of Standards) 70C, no. 4 (1966): 263-273.

Oppenheim, Alan V., and Ronald W. Schaefer. *Digital Signal Processing.* Englewood Cliffs, New Jersey: Prentice-Hall, 1975.

Papoulis, Athanasios. *Probalility, Random Variables, and Stochastic Processes.* New York: McGraw-Hill, 1991.

Skylar, Bernard. *Digital Communications: Fundamentals and Applications.* 2nd. Pearson Education, 2009.

Ward, Chris C., and Karl Iagnemma. "Speed-independent vibration-based terrain classification for passenger vehicles." *Vehicle System Dynamics* (Taylor & Francis Group) 47, no. 9 (September 2009): 1095-1113.

Table 1: The averages and standard deviations of the RIF for the three road segments at different sample rates

	Smooth		**Rough**		**Tracks**	
Rate (Hz)	**Avg. RIF**	**s_{RIF}**	**Avg. RIF**	**s_{RIF}**	**Avg. RIF**	**s_{RIF}**
1	0.136	43.8%	0.264	38.2%	0.404	47.2%
2	0.088	32.1%	0.200	38.8%	0.342	60.0%
4	0.118	21.8%	0.257	25.8%	0.452	23.2%
8	0.145	20.6%	0.299	19.7%	0.539	16.6%
16	0.140	21.4%	0.281	15.7%	0.558	9.2%
32	0.164	25.3%	0.355	14.5%	0.574	9.9%
64	0.151	19.1%	0.342	13.4%	0.553	7.2%
93	0.153	12.9%	0.294	10.0%	0.527	6.8%

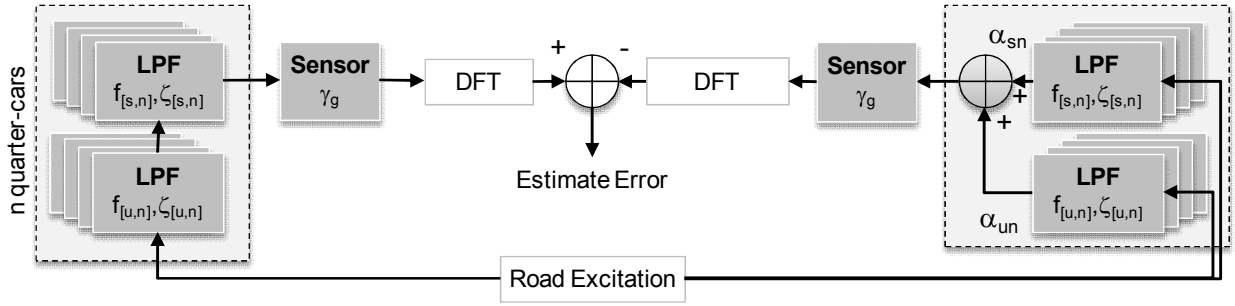

Figure 1. Method of estimating the vehicle mechanical filter parameters

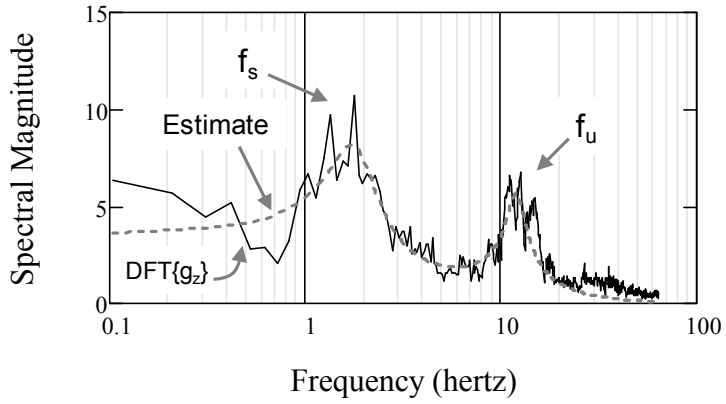

Figure 2. DFT of sensor output versus estimate of mechanical filter response

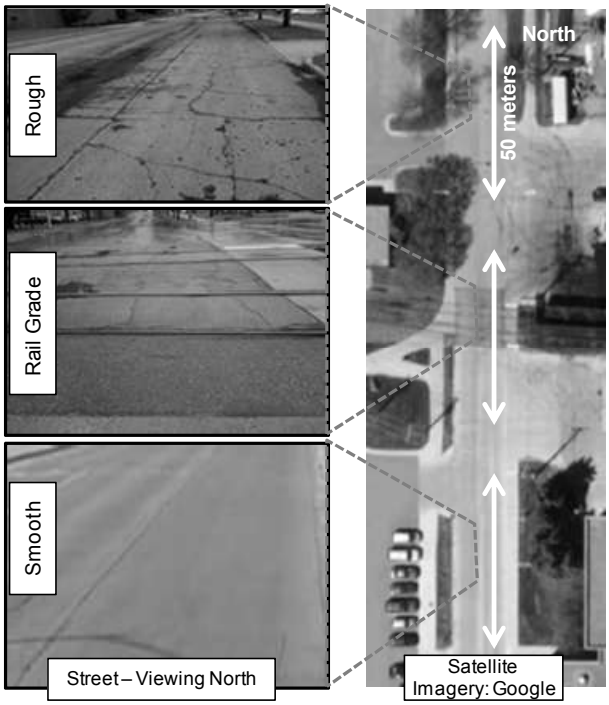

Figure 3. Photographs of Bolley Drive sections analyzed (Imagery: Google)

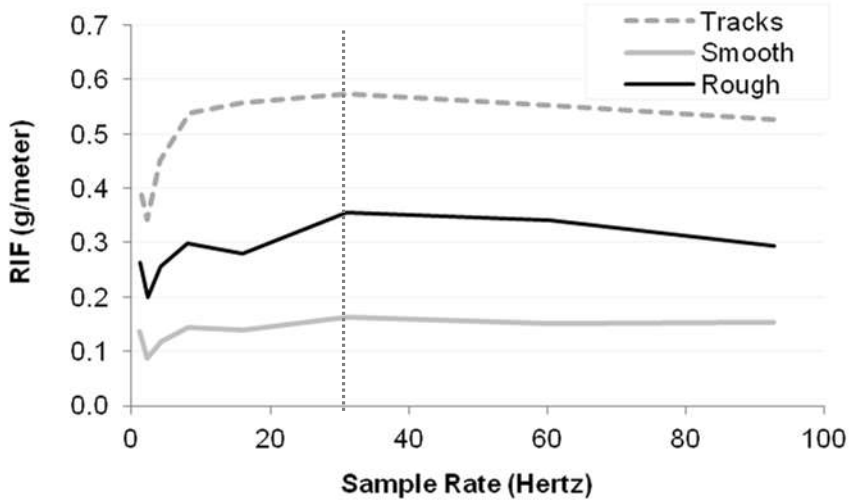

Figure 4. RIF of 50 meter road segments at different sample rates

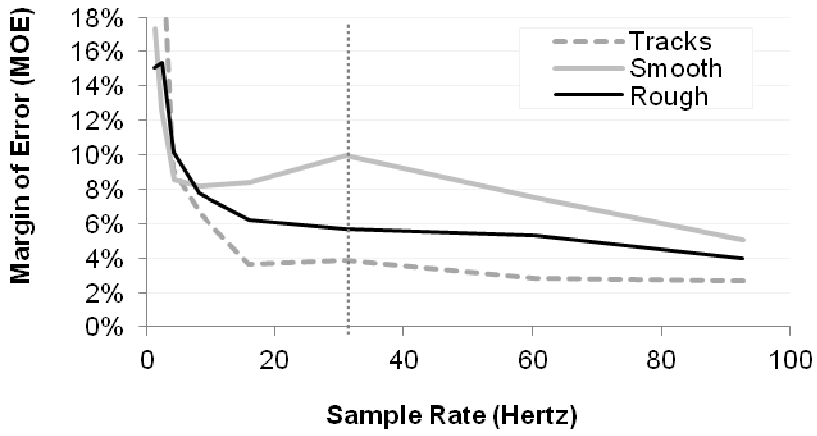

Figure 5. RIF margin-of-error versus sample rate

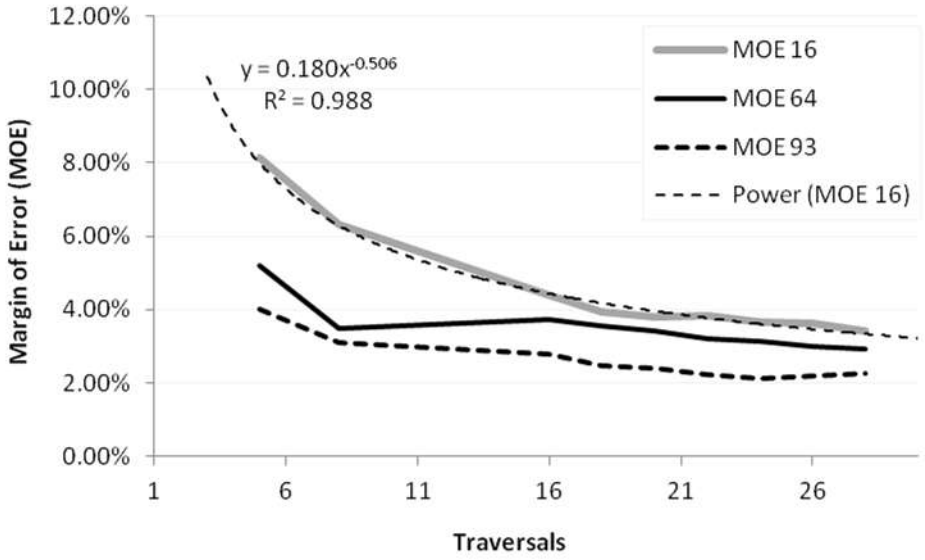

Figure 6. Margin-of-error as a function of traversal volume